RSC Advances

This is an *Accepted Manuscript*, which has been through the Royal Society of Chemistry peer review process and has been accepted for publication.

Accepted Manuscripts are published online shortly after acceptance, before technical editing, formatting and proof reading. Using this free service, authors can make their results available to the community, in citable form, before we publish the edited article. This *Accepted Manuscript* will be replaced by the edited, formatted and paginated article as soon as this is available.

You can find more information about *Accepted Manuscripts* in the Information for Authors.

Please note that technical editing may introduce minor changes to the text and/or graphics, which may alter content. The journal's standard Terms & Conditions and the Ethical guidelines still apply. In no event shall the Royal Society of Chemistry be held responsible for any errors or omissions in this *Accepted Manuscript* or any consequences arising from the use of any information it contains.

ROYAL SOCIETY OF CHEMISTRY

www.rsc.org/advances

Effect of hierarchical hybrid micro/nanorough strontium-loaded surface on osseointegration in osteoporosis

Yongfeng Li [a,1], Qian Fu [a, 1], Yaping Qi [b], Mingming Shen [b], Qiang Niu [a], Kaijin Hu [a,*], Liang Kong [a,*]

[a] State Key Laboratory of Military Stomatology, Department of Oral and Maxillofacial Surgery, School of Stomatology, the Fourth Military Medical University, Xi'an 710032, PR China;

[b] Department of Oral and Maxillofacial Surgery, School of Stomatology, the Second Hospital of Hebei Medical University, Shijiazhuang 050000, PR China.

[1] These authors equally contributed to this study.

Mailing address : Department of Oral and Maxillofacial Surgery, School of Stomatology, the Fourth Military Medical University, 145 West Changle Rd, Xi' an, 710032, P.R.China

***Corresponding author:** Kaijin Hu and Liang Kong

Tel: +86-013630231909; **Fax** : +86-29-84772534;

E-mail: implant@fmmu.edu.cn

RSC Advances Accepted Manuscript

Abstract

This study compared the effect of a hierarchical hybrid micro/nanorough titanium strontium-loaded (MNT-Sr) surface on osseointegration under osteoporotic conditions to those of implants with a smooth titanium surface (ST), microrough titanium surface (MT) etched with hydrofluoric acid (HF), and an NT-Sr surface obtained by magnetron sputtering. The MNT-Sr surface released Sr at a low rate over a long period. In vitro experiments showed that although the MT was the superior surface in terms of promoting bone marrow stromal cells (BMSCs) adhesion and proliferation, the MNT-Sr surface had better biocompatibility for BMSCs differentiation and induced more intercellular junctions than the other surfaces. After 12 weeks of implantation into the distal femurs of ovariectomized rats, MNT-Sr had the highest osseointegration, followed by MT, NT-Sr, and ST surfaces. These results suggest that MNT-Sr combines the advantages of hierarchical micro/nanotopography and Sr to enhance osseointegration in osteoporosis.

Keywords: Strontium, osteoporosis, surface modification, osseointegration, micro, nano

RSC Advances Accepted Manuscript

1. Introduction

Osteoporosis is a skeletal disease characterized by a decrease in bone mass and deterioration of bone microarchitecture, which leads to increased bone fragility and risk of fracture [1]. According to the World Health Organization, there are more than 200 million people worldwide suffering from osteoporosis [2]. Poor bone quantity and quality due to osteoporosis lead to reduced primary stability and inferior osseointegration during prosthetic implantation [3-5]. To improve osseointegration of implants in osteoporosis, previous studies have focused on modifying implant surface roughness as well as drug treatments [6-8].

Modifying implant surface roughness is one of the most effective strategies for enhancing the rate and extent of osseointegration [9]. A micron-scale rough surface prepared by grit blasting followed by acid etching of titanium implants resulted in rapid and increased bone accretion [10]; furthermore, fluoride-modified implants showed increased surface roughness at the nano-level, and improved titanium implant integration into osteoporotic bones [11]. A recent study demonstrated the synergistic effects of a hierarchical micro-/nanotextured surface and micro- and nanotopographies on osteoblast function [12]. Our previous study found that hierarchical micro-/nanotextured surface can also improve titanium implant osseointegration in ovariectomized sheep after 12 weeks [13]. From a biomimetic standpoint, this surface—which is composed of nano-, micro-, and macroscale building blocks assembled in a highly organized manner that simulates natural tissue—is more favorable for promoting osteogenesis around implants than using micro- or nanoscale blocks only [14]. Therefore, implant surfaces with hierarchical micro/nano surface roughness is promising for the treatment of osteoporosis.

Systemic application of anti-osteoporosis drugs—including bisphosphonates and strontium (Sr)—prior to implantation is a common clinical strategy for treating osteoporosis patients [15, 16]. Given serious complications such as the jawbone osteonecrosis associated with bisphosphonate administration [17], Sr is the preferred treatment due to its dual effects of promoting bone formation and reducing bone resorption [18]. Numerous studies have found that systemic Sr administration improved implant osseointegration under osteoporotic conditions [19, 20]; however, some adverse reactions such as toxic epidermal necrolysis and drug rash with eosinophilia, have been reported [21, 22]. Local application of Sr would be expected to circumvent these adverse reactions,and is therefore an ideal strategy for enhancing implant osseointegration.

In this study, an implant surface that aimed to enhance osseointegration in osteoporosis was developed by combining the advantages of hierarchical micro-/nanotopography and Sr surface properties. In vitro and in vivo experiments were carried out to evaluate the bioactivity of the micro/nano Sr-loaded surface with respect to other implant surfaces differing in term of roughness and conjugated chemical elements.

RSC Advances Accepted Manuscript

2. Experimental

2.1 Sample preparation and characterization

Titanium disks (99.99% pure, Φ15×1mm; Zhong Bang Corporation, Xi'an, China) and titanium implants (99.99% pure, Φ1.5×4mm; Zhong Bang Corporation, Xi'an, China)were divided into four groups: smooth titanium (ST); micro titanium (MT) etched with 0.5% (w/v) hydrogen fluoride (HF) for 30 min; nano Sr-loaded titanium (NT-Sr) treated by magnetron sputtering; and micro/nano Sr-loaded titanium (MNT-Sr) etched with HF and subsequently treated by magnetron sputtering. The latter was achieved using an industrial physical vapor deposition system (SKY Technology Development Co. Ltd., Shengyang, China) at 80 W power density, 7200 s deposition time, and 10 cm target-substrate distance, and material deposited from magnetrons. The sintered composite target was made from powdered $SrTiO_3$ with a purity of 99.99%. After sample preparation, disks were ultrasonically cleaned with acetone, followed by ethanol and then deionized water, and then sterilized with irradiated cobalt-60. Samples were characterized by field emission scanning electron microscopy (FE-SEM) (Hitachi S-4800; Tokyo, Japan), atomic force microscopy (AFM) (Innova; Veeco Instruments, Plainview, NY, USA), and energy-dispersive X-ray spectroscopy (EDS) (Hitachi S-4800; Tokyo, Japan), and the hydrophilicity of the samples was measured by surface contact angle measurement (DSA30; Krüss GmbH, Hamburg, Germany).

2.2. Sr release determination

Samples were immersed in 5 ml phosphate-buffered saline (PBS) at 37°C. The average of four samples was calculated to determine each data point. The total volume of PBS was collected using a pipette and replaced with fresh PBS at 1, 4, 7, and 14 days. PBS containing released Sr was analyzed by inductively coupled plasma atomic emission spectrometry (IRIS Advantage ER/S; Thermo Jarrell Ash, Franklin, MA, USA).

2.3. Cell culture

Bone marrow stromal cells (BMSCs) were isolated from femur and tibia bone marrow of 2-week-old Sprague-Dawley rats as previously described [23] in accordance with the rules of the Institutional Animal Care and Use Committee of University. Cells were cultured in α minimum essential medium (α-MEM, Gibco) containing10% fetal bovine serum (Gibco). Cells between passages 2 and 4 were used in experiments. Titanium samples were placed in Costar 24-well plates (Corning Inc., Corning, NY, USA), and cells were seeded at a density of 2×10^4 cells/ml for assays unless otherwise stated.

RSC Advances Accepted Manuscript

2.4. Cell adhesion assay

A total of 2×10^4 cells/ml were seeded on the disks with four different surfaces（n=18; 6 samples were tested at each time point）in each well of a 24-well plate. After incubation for 30, 60, and 120 min, attached cells were stained with 4, 6-diamidino-2-phenylindole (DAPI; Sigma). Images were acquired from five random fields, using a fluorescence microscope (Leica Microsystems, Wetzlar, Germany), and the number of cells in each field was counted.

2.5. Cell proliferation

A 1-ml aliquot of a 2×10^4 cells/ml cell suspension was seeded on the four different surface samples(n=18; 6 samples were tested at each time point) and cultured in α-MEM with 10% bovine calf serum. After 1, 4, and 7 days, cell proliferation was evaluated with the 3-(4, 5-dimethylthiazol-2-yl)-2,5-diphenyltetrazolium bromide (MTT) assay (Sigma, St. Louis, MO, USA). Briefly, at the indicated time points, samples were gently rinsed three times with PBS and transferred to a new plate, and then incubated with MTT solution at 37°C for 4 h. The formazan crystals that formed were dissolved in dimethyl sulfoxide, and the optical density (OD) at 490 nm was measured using a spectrophotometer (BioTek, Winooski, VT, USA).

2.6. Cell morphology

Cell morphology and cell/biomaterial interaction were examined by FE-SEM and confocal laser scanning microscopy (FluoView FV 1000; Olympus, Tokyo, Japan). After incubation for 3 days in α-MEM containing 10% fetal calf serum, the four different surface samples (n=6) with attached cells were fixed in 3% glutaraldehyde, dehydrated in a graded ethanol series, freeze-dried, sputter-coated with gold, and visualized by high-resolution FE-SEM. For fluorescence microscopy, cells cultured for 3 days were fixed in 3.7% formaldehyde solution for 5 min and then permeabilized with 0.1% Triton X-100, followed by incubation with 50 mg/ml fluorescein isothiocyanate (FITC)-phalloidin (Sigma) for 40 min at room temperature in the dark to label actin filaments. Nuclei were stained for 5 min with DAPI.

2.7. ALP activity

Cells (2×10^4/cells/ml) were seeded on the four different surface disks (n=6) and cultured in α-MEM. After 3 days, samples were washed and fixed, and alkaline phosphatase (ALP) staining was carried out for

RSC Advances Accepted Manuscript

30 min using the 5-bromo-4-chloro-3-indolyl-phosphate/nitro blue tetrazolium alkaline phosphatase color development kit (Beyotime Institute of Biotechnology, Shanghai, China). Colorimetry with p-nitrophenyl phosphate as the substrate was used to determine the amount of ALP present.

2.8 Extracellular matrix (ECM) mineralization

ECM mineralization in cells growing on four different surface disks was evaluated by Alizarin Red staining. Cells (2×10^4/ml) were seeded on each disk and cultured for 7 days. After washing with PBS and fixing in 3.7% formaldehyde solution for 1 h, calcium deposits were stained with 2% Alizarin Red S (pH 4.2) (Sigma).

2.9. Animal experiments

2.9.1 Animals and surgical procedures

Procedures were carried out according to the Guidelines for the Care and Use of Laboratory Animals and complied with regulations of the Animal Research Committee of University. Female Sprague-Dawley rats (n = 42; 6 months old; mean weight 330 ± 20 g) were used for experiments. Bilateral ovariectomy (OVX) was performed on 40 animals, while the two remaining rats constituted the sham control group. Bone architecture of the distal femurs of two OVX and the two sham rats was assessed to ensure that the animals were osteoporotic.

In total, 80 implants from the four groups were randomly inserted into the distal femurs of 40 OVX rats (one implant per femur). The surgery was performed under general anesthesia with sodium pentobarbital (40 mg/kg) (Merck, Darmstadt, Germany) administered by intraperitoneal injection. Penicillin (4 WU/kg) was administered for 3 days postoperatively; 12 weeks after implantation, animals were sacrificed for micro-computed tomography (CT) scanning, histological analysis, fluorescence microscopy observation, and biomechanical testing. Calcein (5mg/kg; Sigma Chemicals Co., USA) and tetracycline (25mg/kg; Amresco Ltd., USA) were administered by intraperitoneal injection at 3 and 14 days, respectively, before the rats were sacrificed to determine the period of new bone deposition.

2.9.2 Micro-CT scanning

At 12 weeks after OVX, and prior to biomechanical testing and dehydration for histological analysis, four groups of bone samples (n=10) were scanned by micro-CT (Y. Cheetah; YXLON International GmbH, Hamburg, Germany) at 90 kV, 45 μA, 1000-ms integration time, 450 projections. A three-dimensional

RSC Advances Accepted Manuscript

image was reconstructed with an isotropic voxel size of 15 μm. The multilevel threshold procedure (threshold for bone and implants =500-1200 and >1200, respectively) was applied in order to discriminate bone from other tissues. Images acquired from the scan were used for quantitative analysis. Regions of interest comprising the trabecular compartment around the implant were selected and defined as a ring with a radius of 0.5 mm from the implant surface. Trabecular thickness (Tb.Th), trabecular number (Tb.N), trabecular separation (Tb.Sp), and bone volume/total volume (BV/TV) were determined.

2.9.3. Histological analysis

Half of the bone samples (n=10) in each group were immersed in 75% ethyl alcohol for 7 days, and then dehydrated through a graded series of ethanol and 100% acetone. Samples were embedded in polyester resin and mounted, and 100-μm-thick undecalcified sections were cut using a sawing microtome (Leica SP 1600; Leica Microsystems), with images captured using a fluorescence microscope.

After fluorescence imaging, sections were stained with methylene blue–acid fuchsin and analyzed histometrically using a computer-digitized image analysis system (Leica Imaging Systems, Cambridge, England) coupled to a light microscope (Olympus BH2 with S Plan FL2 lens; Tokyo, Japan) with a high-resolution video camera (CDC/RGB color video camera; Sony, Fujisawa, Japan) and a Sony Trinitron monitor. Bone-to-implant contact (BIC) was determined by calculating as the direct contact interface between bone and implant as a percentage of the total implant interface in the cancellous bone.

2.9.4 Biomechanical testing

Immediately after bone samples were collected, samples (n=10) were used for the biomechanical pull-out test using a universal material testing system (AGS-10KNG; Shimadzu, Kyoto, Japan) at a speed of 2 mm/min. Displacement and force were recorded and used to calculate the maximum pull-out force.

2.10. Statistical analysis

Data were analyzed using SPSS version 16 software (SPSS, Chicago, IL, USA). Comparisons between the OVX and sham groups were performed with the t-test. One-way ANOVA analysis of variance was used for multiple comparisons among the four different groups. Data are expressed as mean ± SD. Differences were considered significant at $P < 0.05$ and highly significant at $P < 0.01$.

RSC Advances Accepted Manuscript

3. Results

3.1 Surface topography, chemical composition, and hydrophilia

The SEM analysis revealed the formation of micropits (diameter: 2–5 μm) on the titanium surface by etching in 0.5% HF acid (Fig. 1). Nanoparticle layers with a diameter of 20–40nm were created by magnetron sputtering, which smoothed the sharp edges of the micro-/nanorough surface, producing uniformly distributed nanoparticles with diameters of 20–40 nm. The roughness of the ST, MT, NT-Sr, and MNT-Sr surfaces measured by AFM differed significantly among groups, as indicated by the surface area diff, root mean square (RMS) roughness, and Z range (Table 1). The chemical composition of samples was analyzed by EDS to determine the surface content of Sr, which was found to be 1.08 ± 0.15 at.% and 1.67 ± 0.27 at.% on the MNT-Sr and NT-Sr surfaces, respectively. The contact angles of water droplets on the ST, MT, NT-Sr, and MNT-Sr surfaces were 46.58° ± 4.43°, 15.90° ± 2.54°, 27.69° ± 5.27°, and 17.03° ± 3.58°, respectively (Fig. 2).

Based on the results of the above analysis, we defined the four different surface groups as follows: ST group with smooth surface; MT group with 2-5 μm micropits on the smooth surface; NT-Sr group with 20-40 nm nanoparticles and Sr loaded on the smooth surface; and MNT-Sr group with 20-40 nm nanoparticles and Sr loaded on the MT surface.

3.2. Sr release

Sr release kinetics were assessed by immersing Sr-containing samples (NT-Sr and MNT-Sr) in 5 ml PBS for up to 14 days. Accumulated Sr release profiles of the samples are shown in Figure 3. The amount of Sr released from the MNT-Sr surface was comparable to but slightly higher point than for NT-Sr at each time point.

3.3. Cell adhesion

The number of adherent BMSCs increased with time for all four groups, but cell numbers were higher on the MT than on the other three surfaces at each time point (Fig. 4). Furthermore, after 60 min of incubation, the number of adherent cells was higher on the MNT-Sr than on the smooth surfaces. Although cell numbers were higher on MNT-Sr than on NT-Sr at 60 and 120 min, the differences were not statistically significant.

3.4. Cell proliferation

The results of the MTT assay showed that cells grown on each surface proliferated over time (Fig. 5). On

RSC Advances Accepted Manuscript

day 1, there was no statistical difference among the groups. On day 4, proliferation rates were similar between MT and NT-Sr; however, by day 7, rates were higher on the MT than on the NT-Sr and MNT-Sr surfaces. Meanwhile, the OD value was significantly higher for the NT-Sr than for the MNT-Sr surface on day 4.

3.5. Cell morphology

3.5.1. SEM

Low magnification micrographs revealed that more BMSCs were attached to the MNT-Sr and MT surfaces after 3 days of incubation (Fig. 6). At higher magnification, the spread of the cells was apparent; moreover, variations in morphology were observed: cells on the ST surface were mainly spindle-shaped and fibroblast-like and were larger than those in other groups. In contrast, cells on the MT and MNT-Sr surfaces were polygonal and had more pseudopodia; on the MNT-Sr surface, these formed intercellular junctions between adjacent cells. BMSCs on NT-Srhad a similar flat, polygonal shape, and intercellular junctions were likewise observed.

3.5.2. Confocal microscopy

BMSCs stained with FITC-phalloidin to label the actin cytoskeleton were visible by confocal microscopy (Fig. 7). A greater number of microfilaments and stress fibers (thick filament bundles) oriented in the same direction were observed in the MNT-Sr group, which were more evenly distributed than in cells on other surfaces. In addition, extensive formation of intercellular junctions was observed on the MNT-Sr surface, and to a lesser degree on the NT-Sr surface. In contrast, although cells on the MT surface extended many filopodia, few intercellular junctions were observed and most cells were aligned in a haphazard orientation Furthermore, the surface topography also affected cytoskeletal morphology, with cells on the MT and MNT-Sr surfaces showing a greater number of stress fibers and actin microfilaments than those on the ST surface.

3.6. ALP activity

Cells grown on MNT-Sr had higher ALP activity after 3 days of culture than those on other surfaces, although there was no statistically significant difference between the NT-Sr and MNT-Sr groups (Fig. 8). Higher ALP activity was observed in cells grown on the NT-Sr as compared to the MT surface. Cells in the MT group had lower ALP activity than those in the ST group, but the difference was not statistically

RSC Advances Accepted Manuscript

significant.

3.7 ECM mineralization

ECM mineralization was evaluated by Alizarin Red staining (Fig. 9). The MNT-Sr surface induced the highest degree of mineralization of the four groups, while NT-Sr was superior to the MT surface in inducing mineralization.

3.8. Micro-CT evaluation

An analysis of bone architecture 12 weeks after OVX revealed that osteoporosis was induced in these rats (Fig. 10 and Table 2). Images reconstructed from the micro-CT scan showed changes in the trabecular bone around the implants (Fig. 11). The bone volume surrounding the implanted MNT-Sr was higher than for other surfaces. BV/TV, Tb.N, and Tb.Th were significantly higher for the MNT-Sr implant; in particular, BV/TV—the most important parameter reflecting bone remodeling—was 0.79-, 0.22-, and 0.39-fold higher than the values for the ST, MT, and NT-Sr surfaces, respectively. A significant difference in Tb.Sp was found only between ST and MT with respect to the MNT-Sr surface. In addition, BV/TV was higher for the MT than for the NT-Sr surface, whereas NT-Sr showed a higher value than ST. Tb.N and Tb.Sp values were similar for NT-Sr and MT surfaces.

3.9. Histological analysis

Osseointegration of the implant into trabecular bone was examined in undecalcified sections stained with Methylene Blue–acid fuchsin (Fig. 12), which distinguishes calcified bone from other tissues by a bright pink color, with implants appearing black [17]. One section from each specimen was analyzed, with the results expressed as BIC (Table 1). After 12 weeks of implantation, the BIC% for ST, MT, NT-Sr, and MNT-Sr was 24.67% ± 3.71%, 38.43% ± 6.42%, 32.69% ± 4.17%, and 51.07% ± 8.09%, respectively. The value for MNT-Sr differed significantly from those of the other three groups; moreover, the BIC% was higher for MT than for ST and NT-Sr. In fluorescence micrographs, tissue was labeled with calcein and tetracycline (visible as green and yellow fluorescence, respectively), which were deposited along implant surfaces. The rate of new bone mineralization, defined as the bone mineralization apposition ratio (MAR, μm/d), was determined from the distance between the two fluorescent markers. MAR differed significantly among the four groups in the order MNT-Sr > NT-Sr > MT > ST ($P < 0.05$).

RSC Advances Accepted Manuscript

3.10. Biomechanical test

The maximum pull-out force for the four surfaces after 12 weeks of implantation is shown in Table 1. MNT-Sr had the highest maximum pull-out force ($P < 0.01$), followed by MT, NT-Sr and ST groups. ($P < 0.01$).

RSC Advances Accepted Manuscript

4. Discussion

Owing to comfort and esthetic considerations, prosthetics with titanium implants are ideal for treating edentulous patients, who are mainly elderly and often suffer from osteoporosis [6], a bone metabolic disease characterized by reduced bone mass and the deterioration of bone microarchitecture. Systemic changes associated with osteoporosis decrease direct contact between bone and the implant – osseointegration [5, 24]. Besides drug treatment, an important clinical strategy for improving implant osseointegration in cases of osteoporosis is to modify implant surface roughness [25].

Surface roughness can be categorized as macro-, micro-, or nano-sized depending on the scale of features [10]. In the present study, a microrough surface was prepared by 0.5% HF etching, as confirmed in SEM images showing micropits with diameters of about 2–5 μm; meanwhile, a nanorough surface was achieved by magnetron sputtering, which produced nanoparticles with diameters of about 20–40 nm. A hierarchical topography with micro-/nanoroughness was achieved by combining the two strategies. A quantitative AFM analysis showed that this surface had superior roughness compared to micro, nano, and smooth surfaces, as measured by surface area diffraction, RMS, and Z range.

The impact of implant roughness in osseointegration under osteoporotic conditions was evaluated by assessing BMSCs bioactivity on different surfaces. In osteoporosis, osteogenesis is inhibited while adipogenesis is induced [26]. For adequate osseointegration, BMSCs differentiation must be biased toward the osteoprogenitor lineage to generate osteoblasts [27]. Our results showed that the MT surface, which has higher hydrophilicity, induced BMSCs adhesion to a greater degree than did NT-Sr and ST surfaces, consistent with a previous report [23]. The highest proliferation rate was observed for BMSCs grown on MT;.however, the NT-Sr surface induced BMSCs differentiation to a greater degree than MT, as evidenced by increased ALP activity and mineralization. Therefore, the higher proliferation rate observed in the MT group reflects BMSCs in an immature and undifferentiated state. Enhanced cell adhesion and proliferation did not promote osteogenesis or mineralization; rather, the coordination of each stage of cellular activation was an important factor for osseointegration [28, 29]. However, the animal experiment yielded contradictory findings: compared to NT-Sr, the MT surface showed higher BIC% and maximal pull-out force. Although nanoroughness increased osteogenic differentiation of BMSCs, it was not sufficient to promote successful osseointegration, which required initial stability provided by micron scale topography and overall implant design, as previously suggested [30]. Thus, a combination of nano- and microroughness can improve osseointegration in osteoporosis.

Various agents including bisphosphonates, raloxifene, and strontium ranelate are used for osteoporosis

RSC Advances Accepted Manuscript

treatment [1]; however, Sr is preferred for its dual effects of promoting bone formation and reducing bone resorption. Nonetheless, Sr can potentially provoke adverse reactions and the systemic effects of long-term Sr usage are undetermined [21, 22]. Thus, local application and a slow rate of release over a long period are desired. In our study, Sr loaded on MNT-Sr and NT-Sr surfaces was released at a slow, uniform rate, demonstrating its advantages in both in vivo and in vitro experiments.

Sr-loaded surfaces (NT-Sr and MNT-Sr) showed two obvious characteristics as compared to surfaces without Sr (ST and MT). Firstly, they induced the formation of intercellular junctions with microfilaments and stress fibers, as compared to cells grown on the respective control surfaces (ST and MT). Increased intercellular contact would likely enhance cellular functions, including differentiation and activation, by coordinating the response to environmental cues. However, since we did not find clear evidence of the positive effects of Sr on intercellular communication, we speculate that the increased intercellular junction observed in cells grown on NT-Sr and MNT-Sr may be due to the nanoscale roughness of these surfaces [31]. Secondly, Sr-loaded surfaces induced greater bone mineralization compared to that observed with the MT surface, consistent with studies demonstrating that Sr induced osteoblastic differentiation and mineralization in cultured BMSCs and also preserved the characteristics and degree of bone mineralization in both osteoporotic and normal monkeys [32, 33]. And the degree of mineralization was essential to the osseointegration which has been demonstrated by previous study [10]. These findings indicate that Sr modulates bone turnover and promotes osteogenesis by inducing bone matrix mineralization, likely via a calcium-sensing receptor-dependent mechanism [34]. In addition, the increased MAR but decreased BIC% in NT-Sr relative to MT, can be attributed to slower Sr release by the former.

Taken together, the above findings suggest that there are at least four essential factors that enhance osseointegration in osteoporosis: (1) initial stability conferred primarily by micron scale topography and overall implant design; (2) coordination of cellular functions including adhesion, proliferation, and differentiation, which are determined by implant-bone interactions; (3) intercellular communication; and (4) enhanced mineralization induced by Sr. In the present study, these factors were integrated to produce a novel hierarchical hybrid micro/nanorough Sr-loaded surface for implants with improved osseointegration in osteoporotic bone.

Although BMSCs adhesion and proliferation were lower for the MNT-Sr than for the MT surface, the Sr-loaded surface induced differentiation to a greater degree. Additionally, animal experiments showed that osseointegration was higher with the MNT-Sr surface, as evidenced by bone formation around the implant, BIC%, and results from the maximum pull-out test, suggesting a synergy between the effects of micro/nano

RSC Advances Accepted Manuscript

scale roughness and Sr loading. The biomimetic properties of MNT-Sr also enhance osseointegration. Bone tissue is assembled in a highly organized manner and is composed of nano- (non-collagenous organic proteins, fibrillar collagen, and hydroxyapatite crystals), micro- (lamellae, osteons, and Haversian systems), and macroscale (cancellous and cortical bones) building blocks [14]. As such, compared to the other surfaces, the hierarchical hybrid micro-/nanorough surface can better mimic natural bone structure and ECM, and thereby provides a more suitable topography for cell functions, while mineralization was promoted by the presence of Sr on the surface.

RSC Advances Accepted Manuscript

5. Conclusion

This study had some limitations, including the short observation time and measured parameters. Moreover, the effects of nanoroughness and Sr loading could not be precisely established, since surface roughness and chemical modification were simultaneously achieved by magnetron sputtering. Nonetheless, we can conclude from our results that the MNT-Sr surface modified by HF acid etching and magnetron sputtering can improve titanium implant osseointegration under osteoporotic conditions owing to the synergistic effects of micro-/nanoscale roughness and Sr loading. The different surfaces used in this study may have favour osseointegration in the following ways: a smooth surface induced the spreading of the cells;a micro surface was beneficial for cell adhesion; a nano surface stimulated proliferation and differentiation; an Sr-loaded surface resulted in better bone mineralization; and the synergistic effects of nanoscale roughness and Sr loadingpromoted intercellular communication.

RSC Advances Accepted Manuscript

6. Acknowledgements

This work was supported by the National Natural Science Foundation of China (Nos. 81371186) and Innovation Research Team in University (No. IRT 13051).

RSC Advances Accepted Manuscript

References:

1 T. D. Rachner and S. Khosla and L. C. Hofbauer, *Lancet*., 2011, 377, 1276-1287.

2 T. Willson, S. D. Nelson, J. Newbold, R. E. Nelson, and J. LaFleur, *Clin. Epidemiol.,* 2015, 7, 65-76.

3 H. Chen, N. Liu, X. Xu, X. Qu, and E. Lu, *PLoS One.,* 2013, 8, 71955.

4 J. Otomo-Corgel, *Periodontol. 2000.,* 2012, 59, 111-139.

5 F. Marco, F. Milena, G. Gianluca, and O. Vittoria, *Micron.,* 2005, 36, 630-644.

6 A. Mellado-Valero, J. C. Ferrer-Garcia, J. Calvo-Catala, and C. Labaig-Rueda, *Med. Oral. Patol. Oral. Cir. Bucal.,* 2010, 15, 52-57.

7 W. Zhang, Y. Jin, S. Qian, J. Li, Q. Chang, D. Ye, H. Pan, M. Zhang, H. Cao, X. Liu, and X. Jiang, *Nanomedicine.,* 2014, 10, 1809-1818.

8 X. Li, Y. Li, Y. Liao, J. Li, L. Zhang, and J. Hu, *Int. J. Oral. Maxillofac. Implants .,* 2014, 29, 196-202 .

9 L. Le Guehennec, A. Soueidan, P. Layrolle, and Y. Amouriq, *Dent. Mater.,* 2007, 23, 844-854.

10 G. Mendonca, D. B. Mendonca, F. J. Aragao, and L. F. Cooper, *Biomaterials.,* 2008, 29, 3822-3835.

11 Y. Li, S. Zou, D. Wang, G. Feng, C. Bao, and J. Hu, *Biomaterials.,* 2010, 31, 3266-3273.

12 L. Zhao, S. Mei, P. K. Chu, Y. Zhang, and Z. Wu, *Biomaterials.,* 2010, 31, 5072-5082.

13 J. Xiao, H. Zhou, L. Zhao, Y. Sun, S. Guan, B. Liu, and L. Kong, *Osteoporos. Int.,* 2011, 22, 1907-1913.

14 J. Y. Rho, L. Kuhn-Spearing and P. Zioupos, *Med. Eng. Phys.,* 1998, 20, 92-102.

15 S. Memon, R. L.Weltman, and J. A. Katancik, *Int. J. Oral. Maxillofac. Implants.,* 2012, 27, 1216-1222.

16 L. Maimoun, T. C. Brennan, I. Badoud, V. Dubois-Ferriere, R. Rizzoli, and P. Ammann, *Bone.,* 2010, 46, 1436-1441

17 A. A. Fernandez, F. Herion, E. Rompen, J. Y. Reginster, M. Magremanne, and F. Lambert, *J. Clin. Periodontol.,* 2015, 190-195.

18 N. S. Pors, *Bone.,* 2004, 583-588.

19 Y. Li, X. Li, G. Song, K. Chen, G. Yin, and J. Hu, *Clin. Oral. Implants. Res.,* 2012, 1038-1044.

20 Y. Li, G. Feng, Y. Gao, E. Luo, X. Liu, and J. Hu, *J. Orthop. Res.,* 2010, 28, 578-582.

21 H. Y. Lee, D. Lie, K. S. Lim, T. Thirumoorthy, and S. M. Pang, *Osteoporos. Int.,* 2009, 20, 161-162.

22 A. P. Jonville-Bera, B. Crickx, L. Aaron, I. Hartingh, and E. Autret-Leca, *Allergy.,* 2009, 64, 658-659.

23 J. Wang, Y. An, F. Li, D. Li, D. Jing, T. Guo, E. Luo, and Ma, C, *Acta. Biomater.,* 2014, 10,975-985 .

24 A. Piattelli, A. E. Pontes, M. Degidi, and G. Iezzi, *Dent. Mater.,* 2011, 27, 53-60.

25 DM. Ehrenfest. Dohan, P. G. Coelho, B. S. Kang, Y. T. Sul, and T. Albrektsson, *Trends Biotechnol.,* 2010, 28, 198-206.

26 A. M. Pino, C. J. Rosen and J. P. Rodriguez, *Biol. Res.*, 2012, 45, 279-287.

27 R. Tasso, F. Fais, D. Reverberi, F. Tortelli, and R. Cancedda, *Biomaterials.,* 2010, 31, 2121-2129.

28 R. Civitelli, *Arch. Biochem. Biophys.,* 2008, 473, 188-192.

29 P. C. Schiller, G. D'Ippolito, W. Balkan, B. A. Roos, and G. A. Howard, *Bone.,* 2001, 28, 38-44.

30 L. Meirelles, A. Arvidsson, T. Albrektsson, and A. Wennerberg, *Clin. Oral. Implants. Res.,* 2007, 18, 326-332.

31 L. Zhao, L. Liu, Z. Wu, Y. Zhang, and P. K. Chu, *Biomaterials.,* 2012, 33, 2629-2641.

32 W. Querido, A. P. Campos, F. E. Martins, G. R. San, A. M. Rossi, and M. Farina, *Cell. Tissue. Res.,* 2014, 357, 793-801.

33 D. Farlay, G. Boivin, G. Panczer, A. Lalande, and P. J. Meunier, *J. Bone. Miner. Res.,* 2005, 20, 1569-1578.

34 S. Takaoka, T. Yamaguchi, S. Yano, M. Yamauchi, and T. Sugimoto, *Horm. Metab. Res.,* 2010, 42, 627-631.

RSC Advances Accepted Manuscript

Tables

Table 1. Roughness values and maximum pull-out force of various implanted surfaces

Parameters	Groups			
	ST	MT	NT-Sr	MNT-Sr
Surface area diffraction (%)	7.03 ± 3.28	25.42 ± 3.45**	21.38 ± 0.60** ##	31.68±5.54** # ††
RMS (nm)	24.1 ± 5.16	55.85 ± 8.77**	39.99 ± 11.62** ##	64.55±5.17** # ††
Z range (nm)	241.25 ± 60.23	567.75 ± 76.81**	459.25 ± 83.53** ##	646.00±80.37** # ††
Maximum pull-out force (N)	37.1 ± 5.4	67 ± 8.59**	56.3 ± 9.76** ##	91.1±8.05** ## ††

ST, smooth titanium surface; MT, micro titanium surface; NT-Sr, micro/nano Sr-containing titanium surface; MNT-Sr, micro/nano Sr-containing titanium surface; RMS, root mean square roughness. **P < 0.01 vs. ST; #P < 0.05, ##P < 0.01 vs. MT; ††P < 0.01 vs. NT-Sr.

Table 2. Bone architecture parameters in rats 12 weeks after OVX

Parameter	Groups	
	Sham	OVX
BV/TV (%)	46.81 ± 5.79	19.06 ± 3.34**
Tb.N (mm^{-1})	7.25 ± 0.36	3.52 ± 0.77**
Tb.Th (μm)	58.67 ± 3.99	25.00 ± 5.60**
Tb.Sp (μm)	97.25 ± 20.66	300.19 ± 71.47**

BV/TV, bone volume/total volume; Tb.N, trabecular number; Tb.Th, trabecular thickness; Tb.Sp, trabecular separation; OVX, bilateral ovariectomy.

**P < 0.01 vs. Sham.

RSC Advances Accepted Manuscript

Figure captions

Figure 1. Titanium surfaces used in this study. Disks are shown in the top panels, and images acquired by scanning electron microscopy (SEM) and atomic force microscopy (AFM) in the middle and lower panels, respectively, show the surface topography of each disk. ST, smooth titanium surface; MT, micro titanium surface; NT-Sr, micro/nano Sr-containing titanium surface; MNT-Sr, micro/nano Sr-containing titanium surface. (n=8)

Figure 2. Surface hydrophilicity as determined by surface contact-angle measurement. Surfaces are as indicated in the legend for Figure 1. (n=8)

Figure 3.

Accumulated Sr release as determined by inductively coupled plasma atomic emission spectrometry. NT-Sr, micro/nano Sr-containing titanium surface; MNT-Sr, micro/nano Sr-containing titanium surface. (n=20, 5 samples were tested at each time point)

Figure 4. Initial number of bone marrow stromal cells adhering to various surfaces. Cells were stained with 4,6-diamidino-2-phenylindole and counted after incubation with disks for the indicated times. Surfaces are as indicated in the legend for Figure 1. $^{*}P < 0.05$, $^{**}P < 0.01$ vs. ST; $^{\#}P < 0.05$, $^{\#\#}P < 0.01$ vs. MT; $^{\dagger}P < 0.05$, $^{\dagger\dagger}P < 0.01$ vs. NT-Sr. (n=18; 6 samples were tested at each time point.)

Figure 5. Bone marrow stromal cell proliferation after incubation on various surfaces for indicated times. Surfaces are as indicated in the legend for Figure 1. $^{*}P < 0.05$, $^{**}P < 0.01$ vs. ST; $^{\#}P < 0.05$, $^{\#\#}P < 0.01$ vs. MT; $^{\dagger}P < 0.05$, $^{\dagger\dagger}P < 0.01$ vs. NT-Sr. (n=18; 6 samples were tested at each time point.)

Figure 6. Scanning electron micrographs of bone marrow stromal cell adhesion on various surfaces after a 3-day incubation. Surfaces are as indicated in the legend for Figure 1. (n=6)

Figure 7. Confocal micrographs of bone marrow stromal cells adhering to various surfaces. Surfaces are as indicated in the legend for Figure 1. Cells were stained with 4,6-diamidino-2-phenylindole (blue) and fluorescein isothiocyanate-phalloidin (green) to visualize nuclei and actin filaments, respectively.(n=6)

RSC Advances Accepted Manuscript

Figure 8. Alkaline phosphatase (ALP) activity of bone marrow stromal cells cultured for 3 days on various surfaces. Surfaces are as indicated in the legend for Figure 1. ALP activity was calculated as a percentage of tricalcium phosphate (TCP). *P < 0.05, **P < 0.01 vs. ST; $^{\#}$P < 0.05, $^{\#\#}$P < 0.01 vs. MT. (n=6)

Figure 9. Extracellular matrix mineralization in bone marrow stromal cells cultured on various surfaces for 7 days. Surfaces are as indicated in the legend for Figure 1. Mineralization was determined by Alizarin Red staining.

Figure 10. Micro-computed tomography images of femoral bone in a rat model of osteoporosis (OP).

Figure 11. Micro-computed tomography analysis of changes in bone architecture around various implant surfaces. Surfaces are as indicated in the legend for Figure 1. BV/TV, bone volume/total volume; Tb.N, trabecular number; Tb.Th, trabecular thickness; Tb.Sp, trabecular separation. (n=10)

Figure 12. Histological analysis of mineralization and osseointegration around various implant surfaces. Surfaces are as indicated in the legend for Figure 1. (Top) Bone tissue was identified by Methylene Blue–acid fuchsin staining. New bone deposition was determined by administering calcein (green) and tetracycline (yellow) by intraperitoneal injection to rats 3 and 14 days, respectively, before sacrifice. (Bottom) Mineralization and osseointegration were determined by bone mineralization apposition ratio (MAR) and bone-to-implant contact (BIC), respectively. (n=10)

RSC Advances Accepted Manuscript

Figure 1

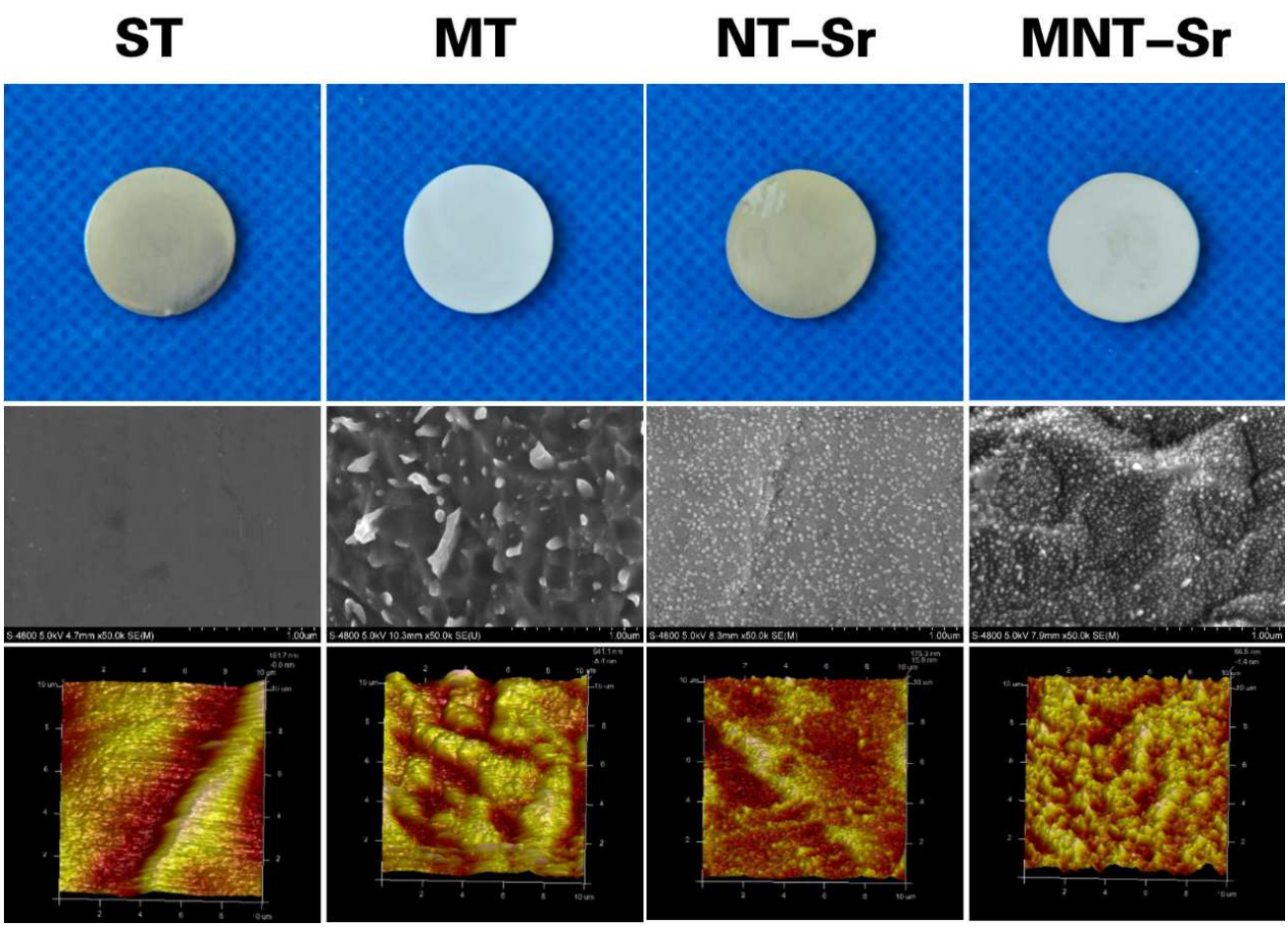

RSC Advances Accepted Manuscript

Figure 2

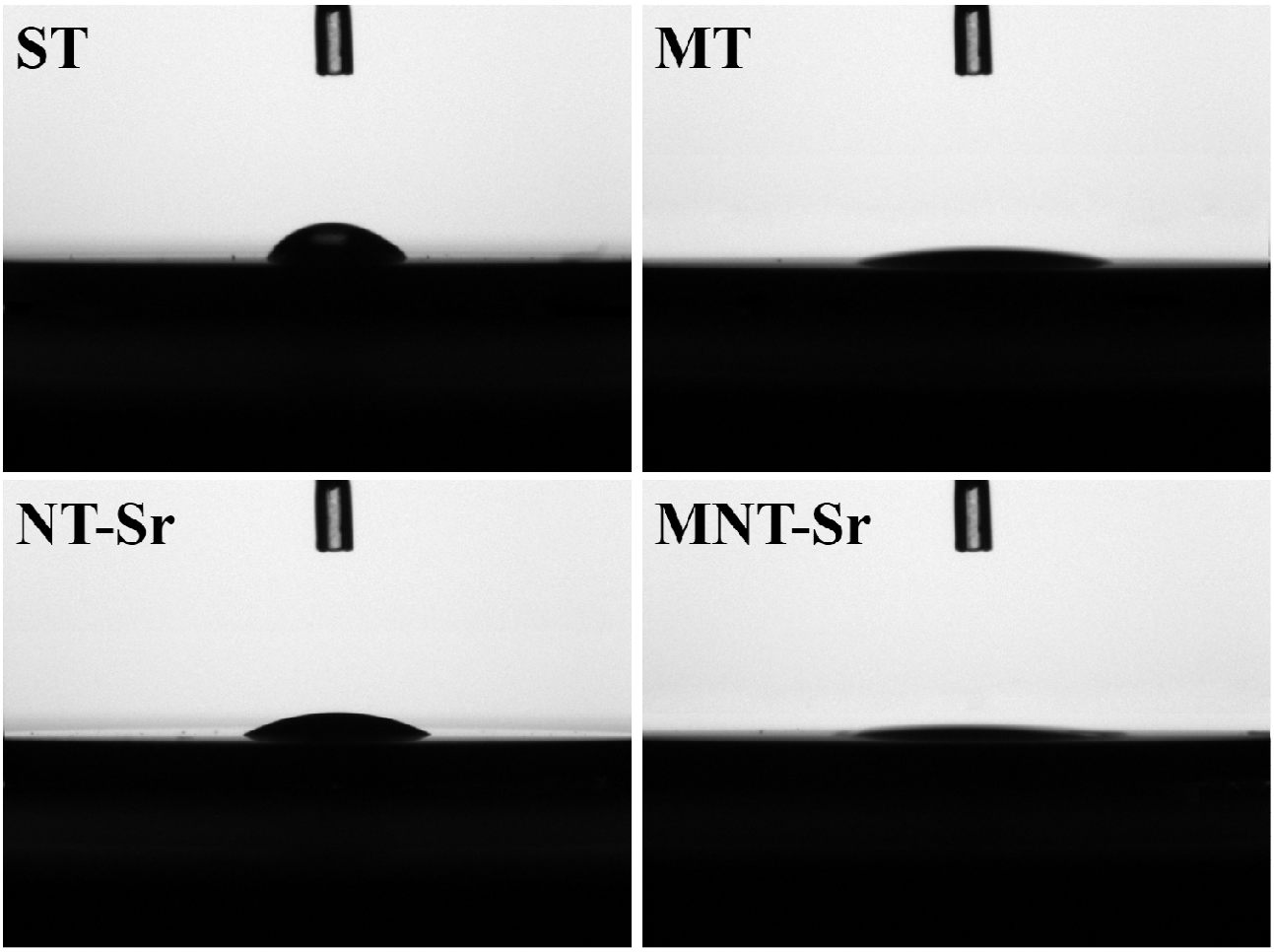

RSC Advances Accepted Manuscript

Figure 3

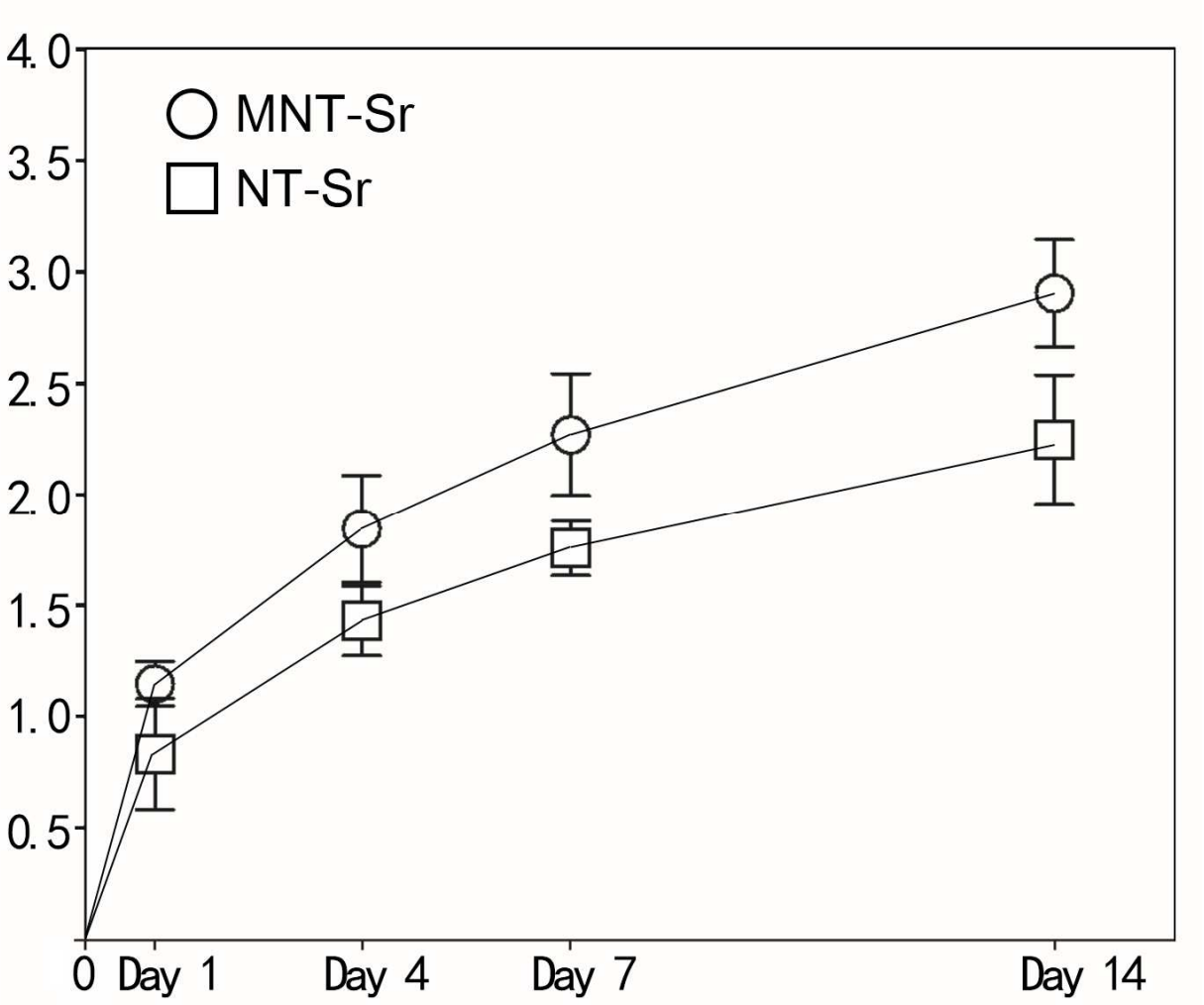

RSC Advances Accepted Manuscript

Figure 4

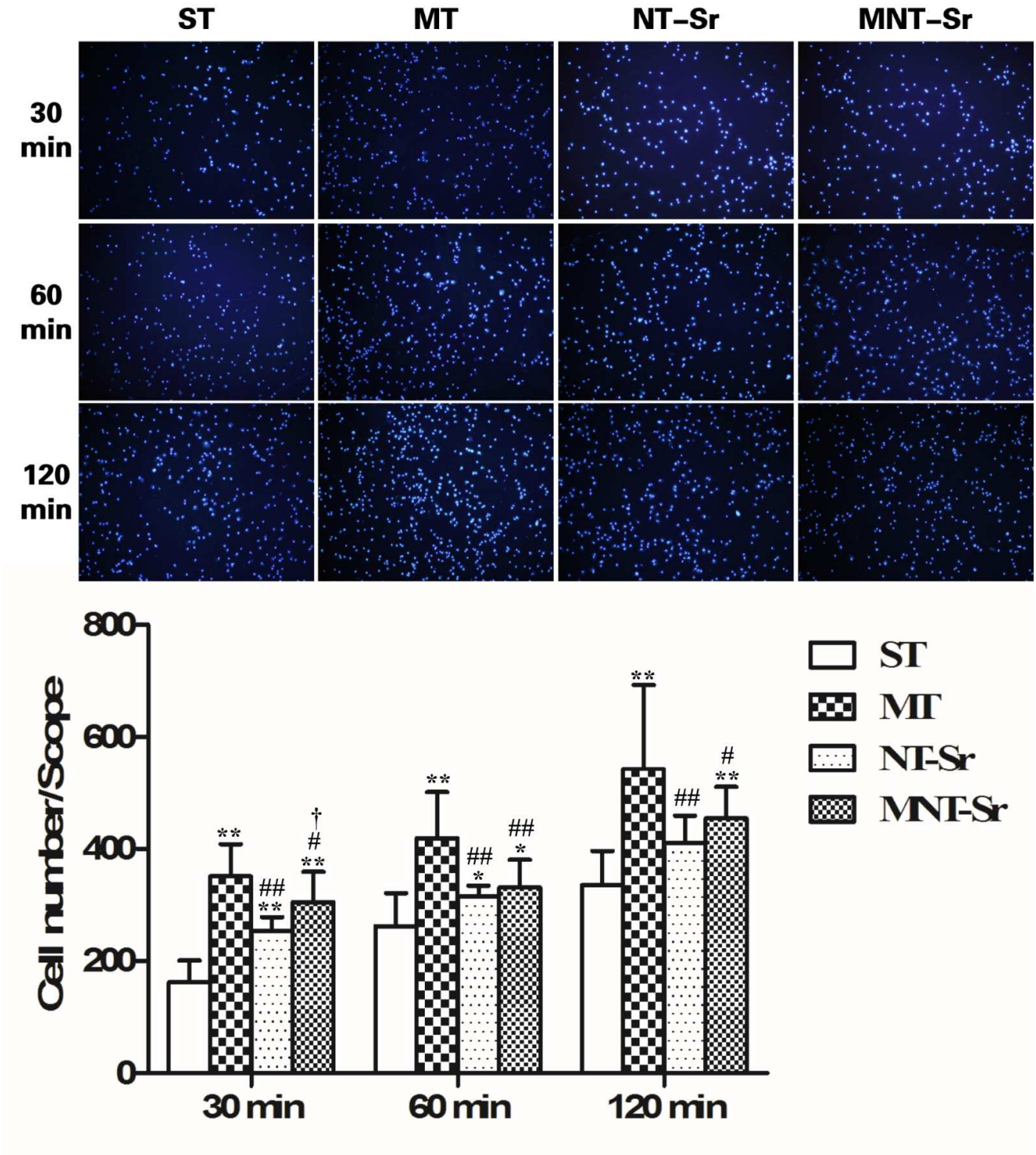

RSC Advances Accepted Manuscript

Figure 5

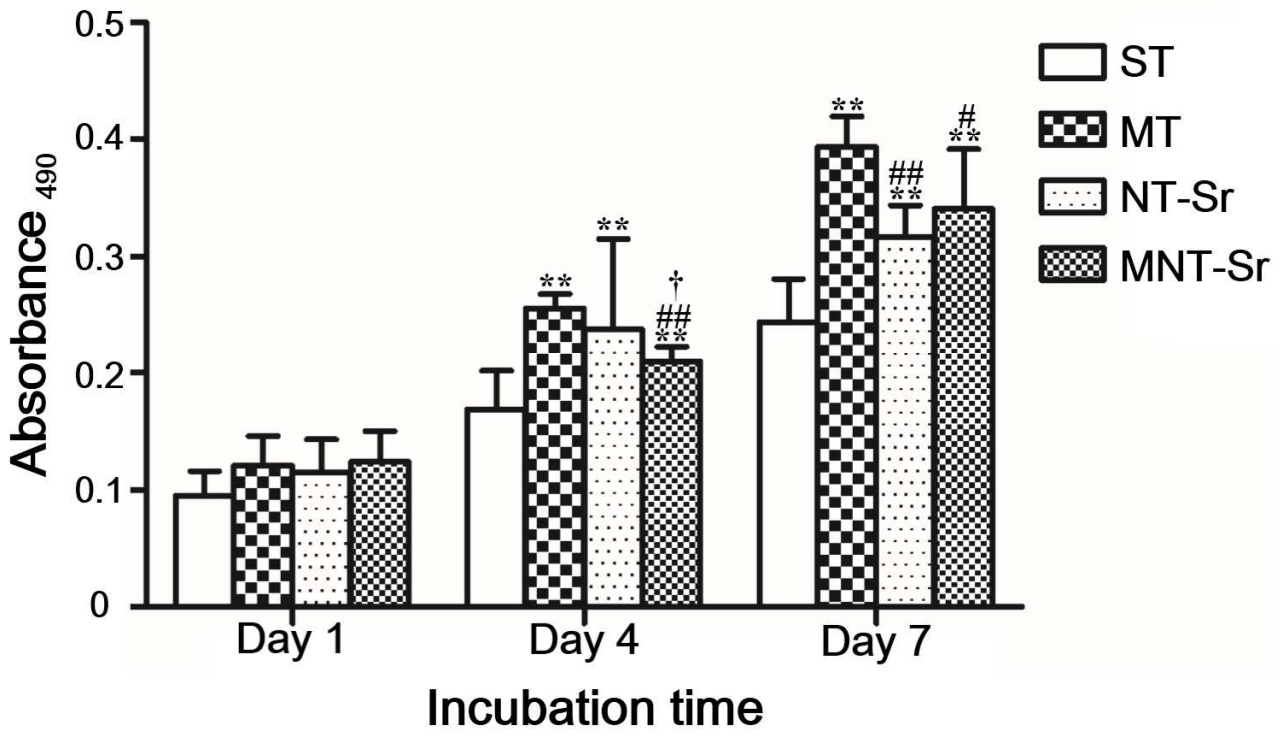

RSC Advances Accepted Manuscript

Figure 6

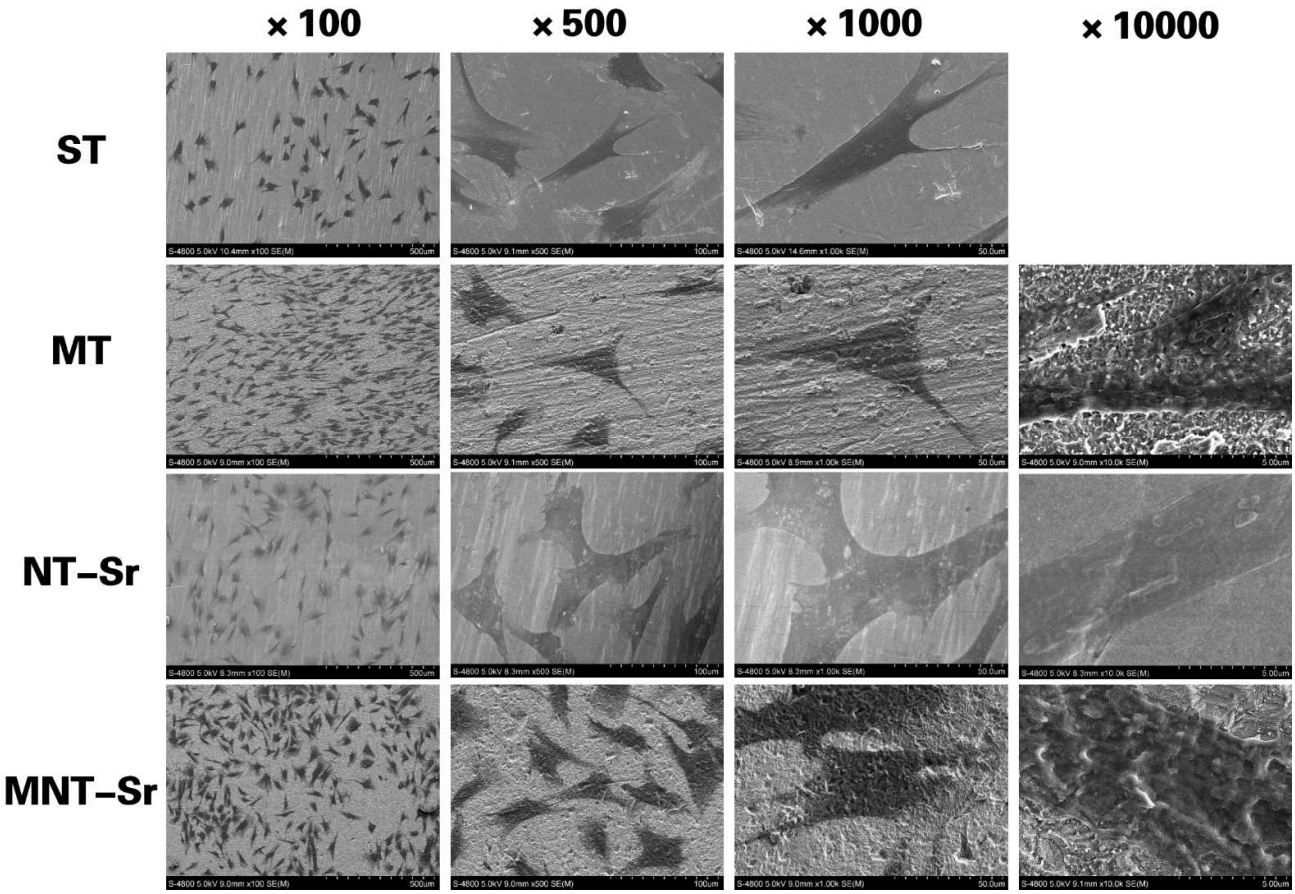

RSC Advances Accepted Manuscript

Figure 7

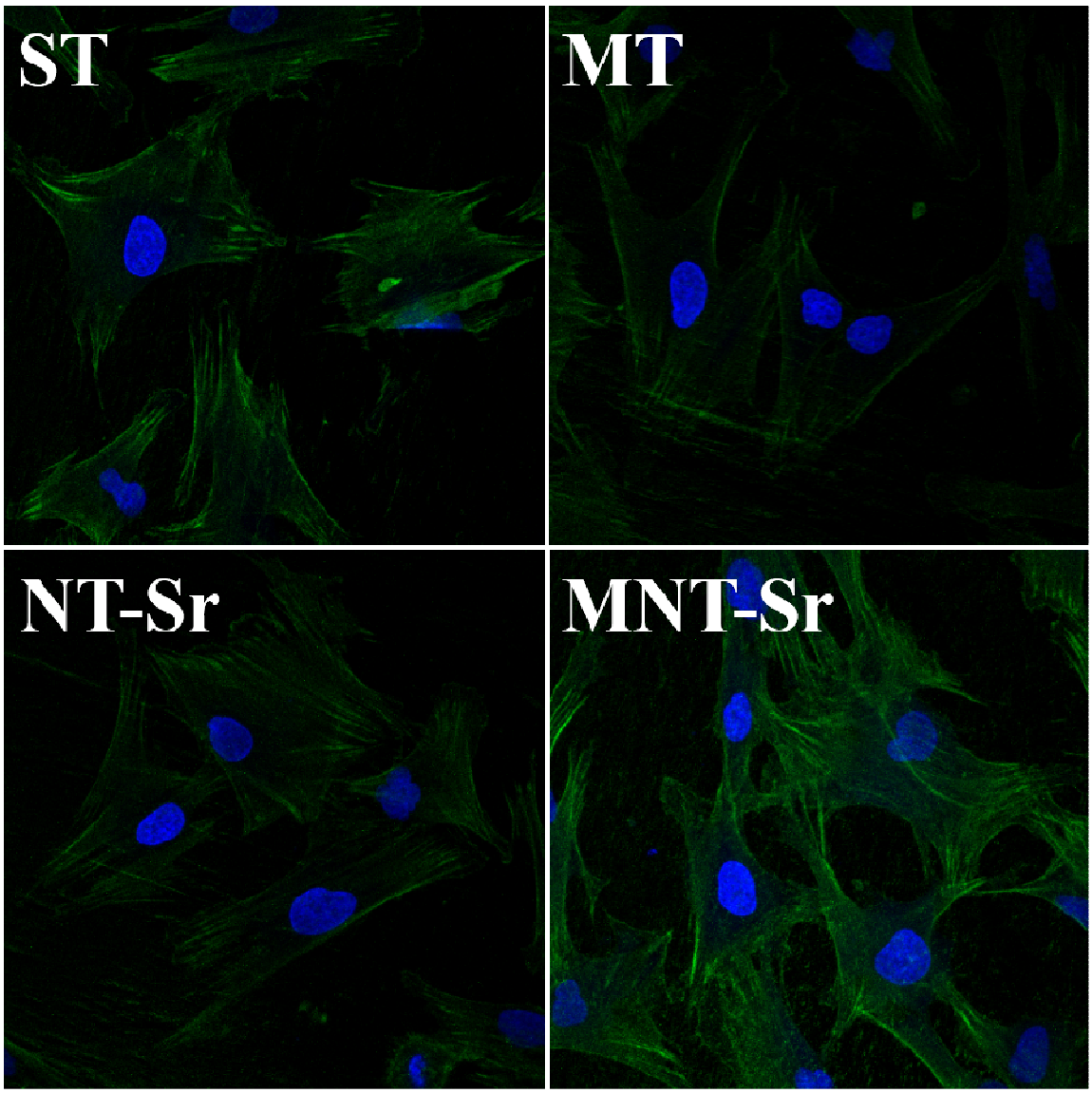

RSC Advances Accepted Manuscript

Figure 8

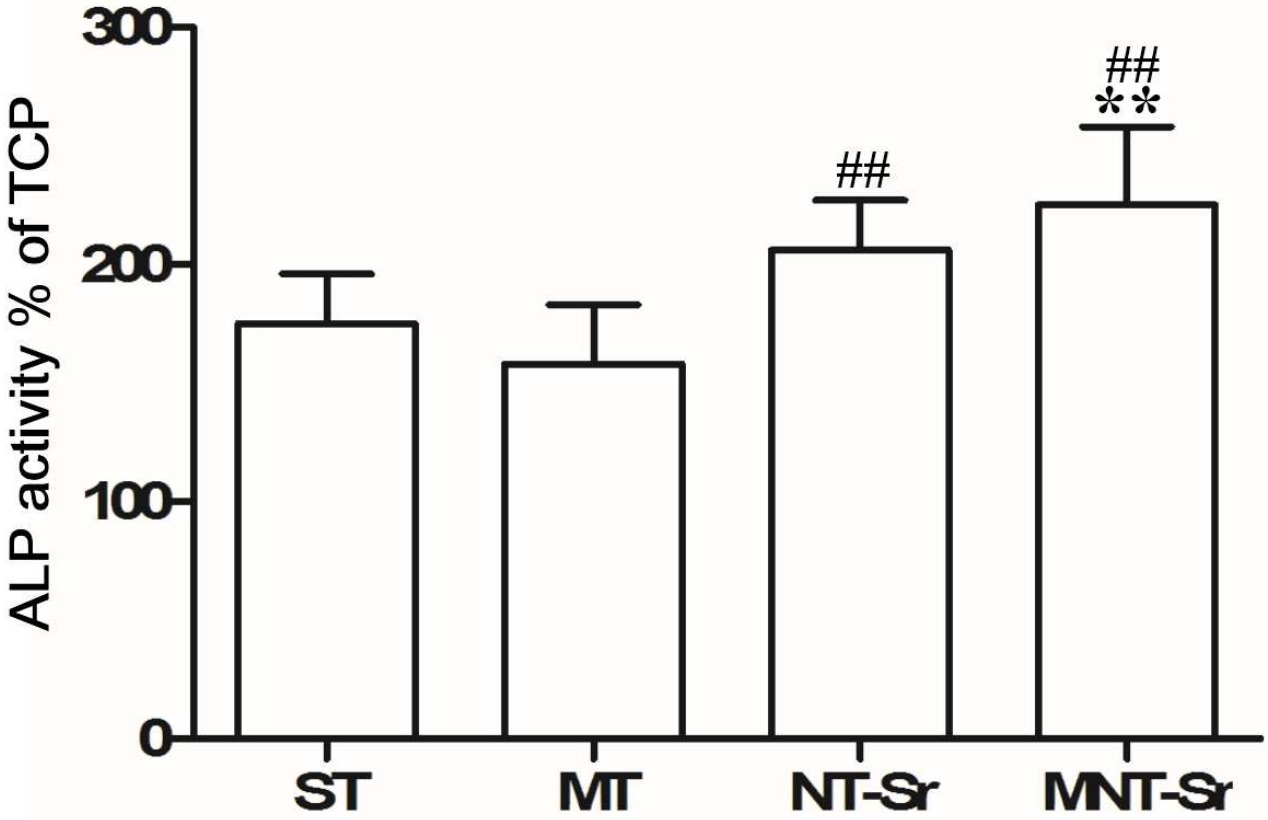

RSC Advances Accepted Manuscript

Figure 9

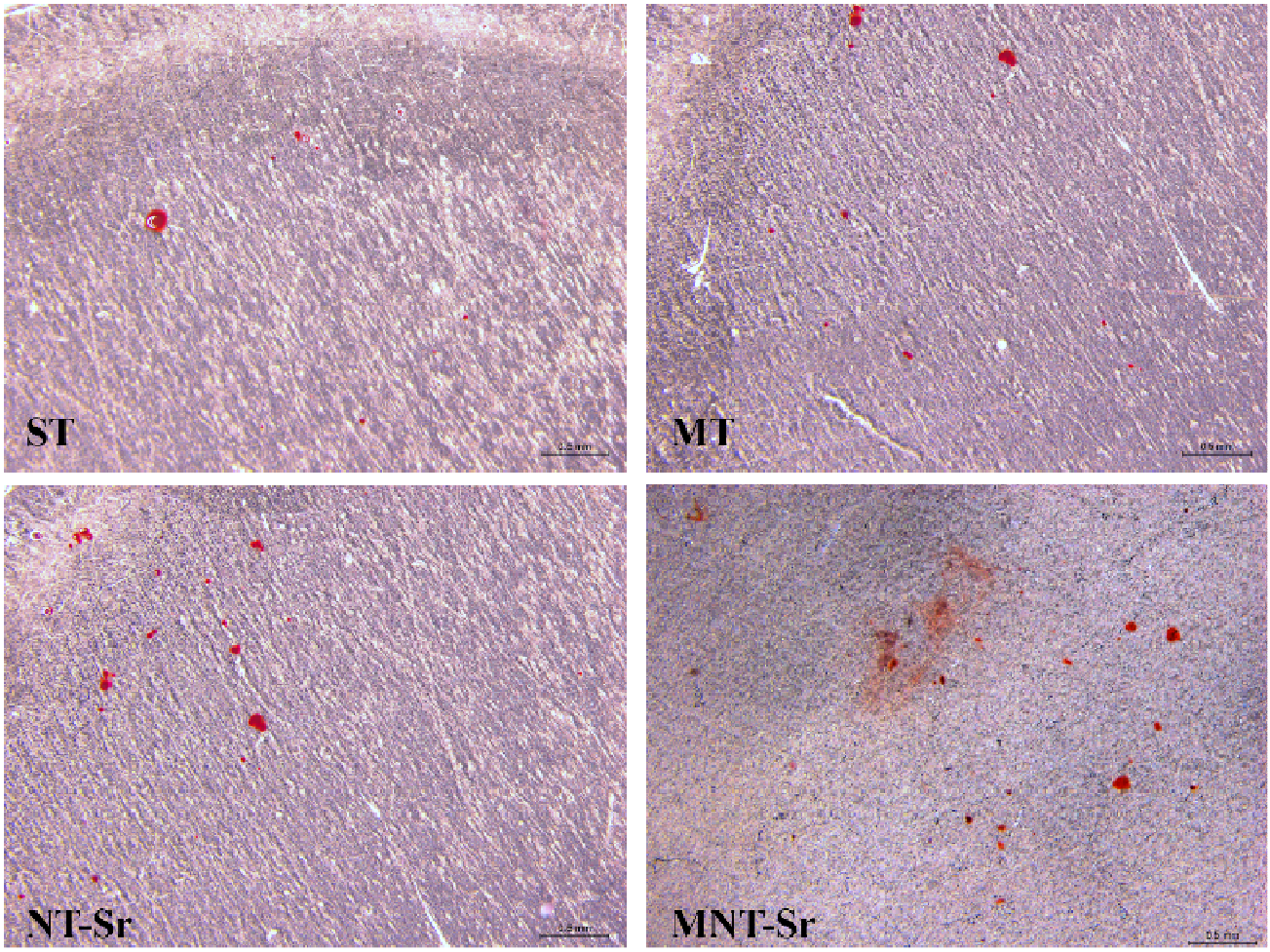

RSC Advances Accepted Manuscript

Figure 10

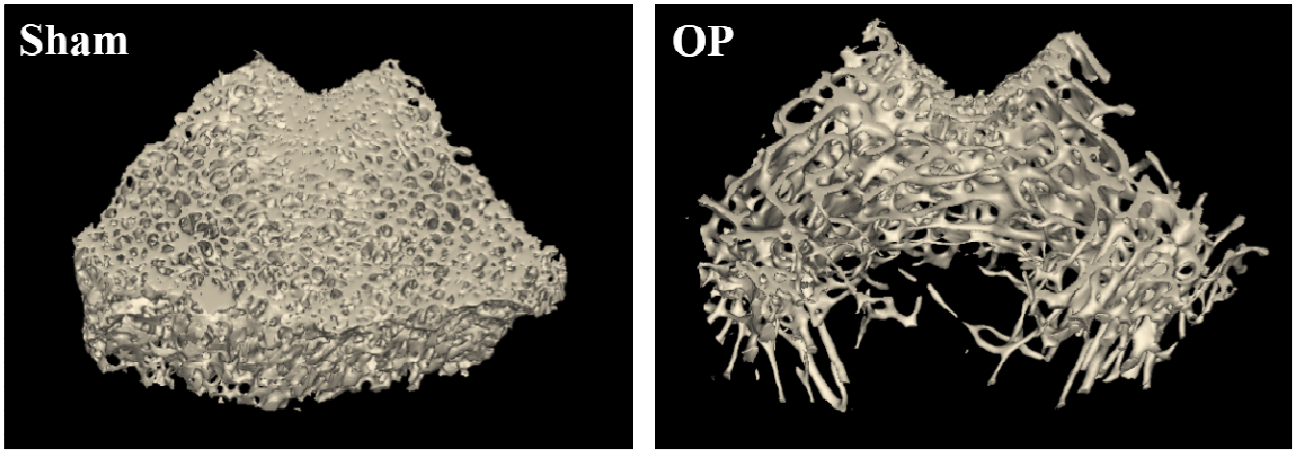

RSC Advances Accepted Manuscript

Figure 11

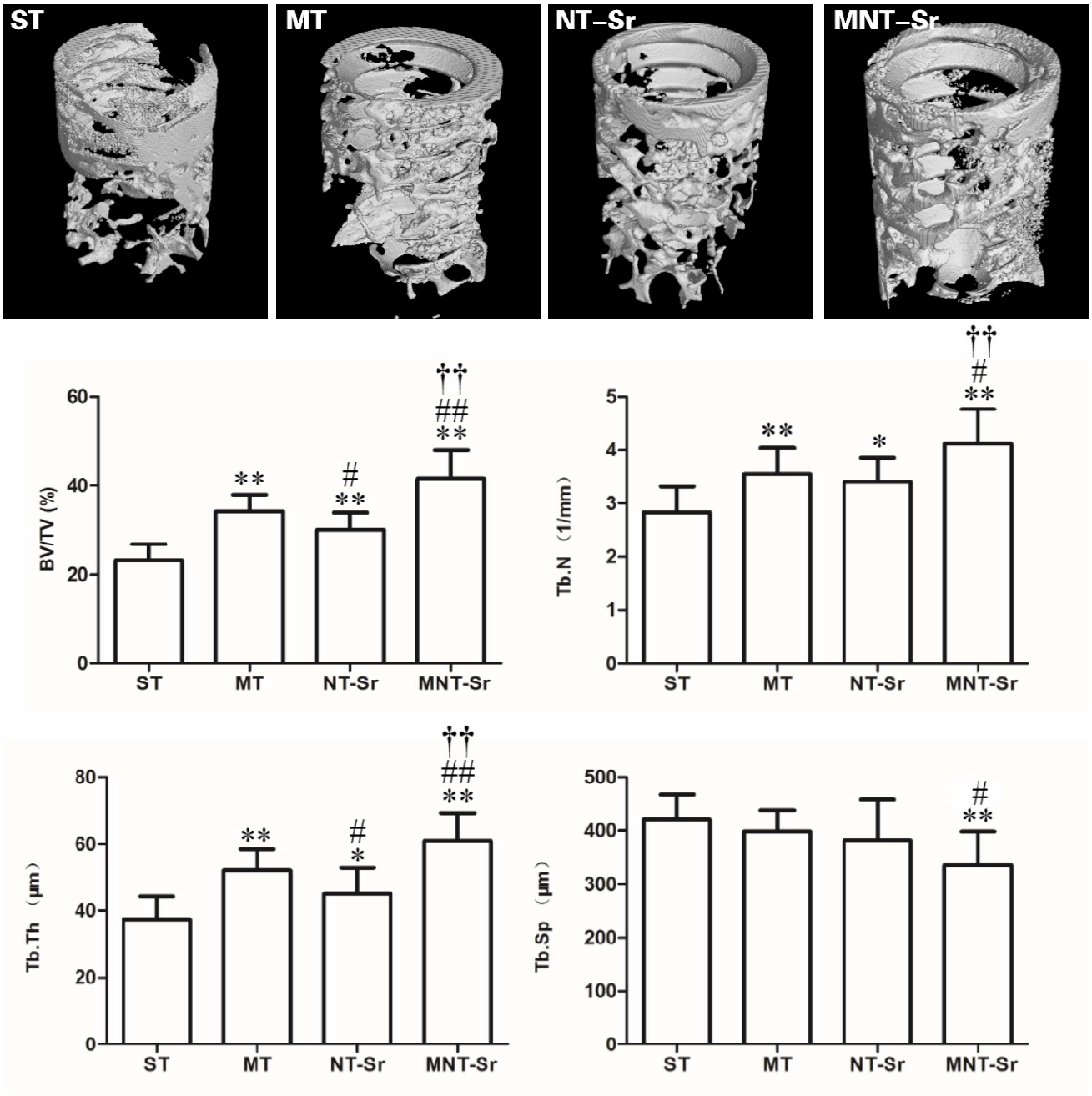

RSC Advances Accepted Manuscript

Figure 12

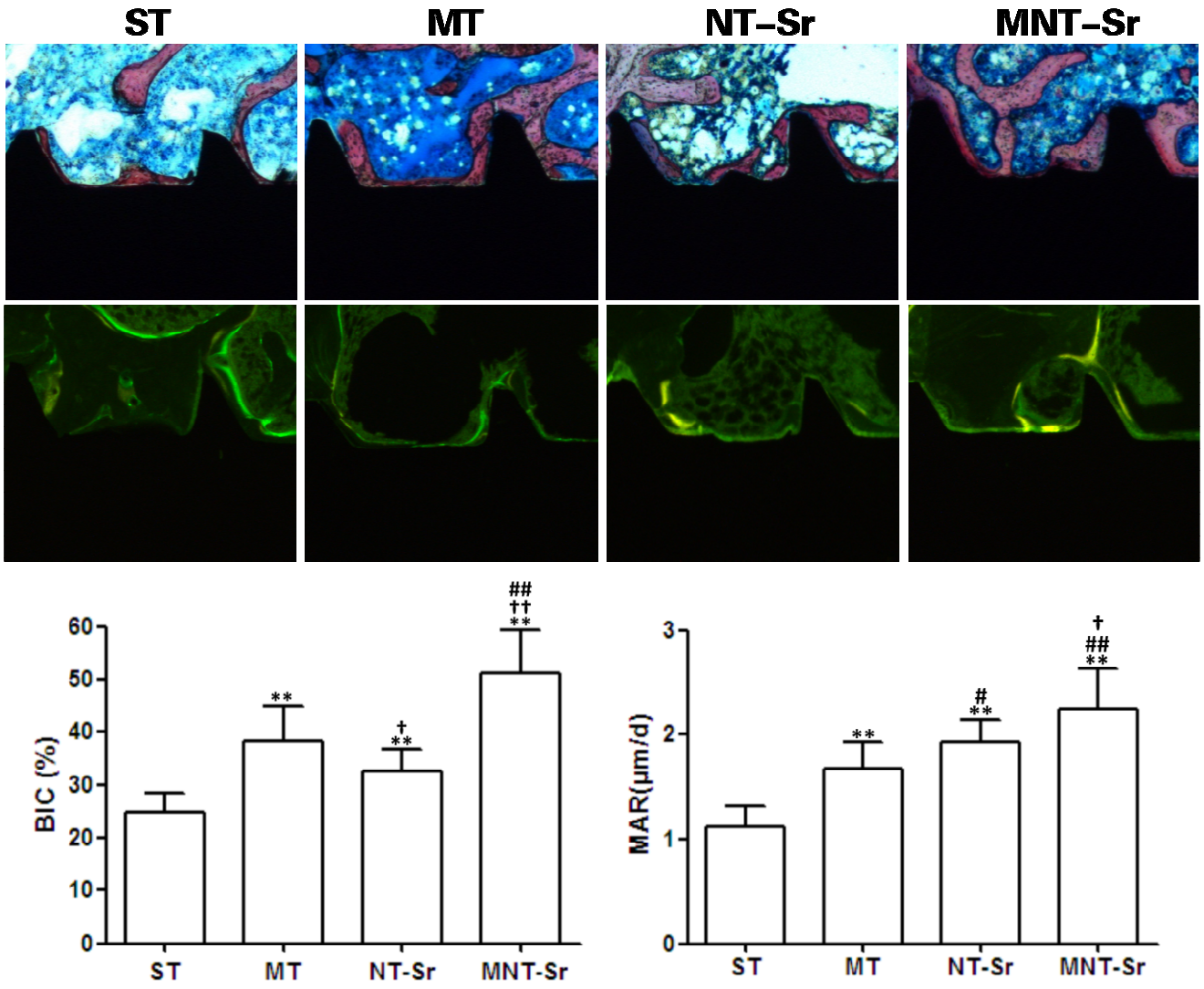

RSC Advances Accepted Manuscript